Geophys. J. Int. (2007) **169,** 271–280 doi: 10.1111/j.1365-246X.2006.03303.x

Extraction of near-surface properties for a lossy layered medium using the propagator matrix

K. Mehta,[1] R. Snieder[1] and V. Graizer[2]

[1] *Center for Wave Phenomena, Department of Geophysics, Colorado School of Mines, Golden, CO* 80401, *USA. E-mail: kmehta@dix.mines.edu*
[2] *California Geological Survey, Sacramento, CA* 95814, *USA*

Accepted 2006 November 16. Received 2006 November 12; in original form 2006 May 1

SUMMARY

Near-surface properties play an important role in advancing earthquake hazard assessment. Other areas where near-surface properties are crucial include civil engineering and detection and delineation of potable groundwater. From an exploration point of view, near-surface properties are needed for wavefield separation and correcting for the local near-receiver structure. It has been shown that these properties can be estimated for a lossless homogeneous medium using the propagator matrix. To estimate the near-surface properties, we apply deconvolution to passive borehole recordings of waves excited by an earthquake. Deconvolution of these incoherent waveforms recorded by the sensors at different depths in the borehole with the recording at the surface results in waves that propagate upwards and downwards along the array. These waves, obtained by deconvolution, can be used to estimate the *P*- and *S*-wave velocities near the surface. As opposed to waves obtained by cross-correlation that represent filtered version of the sum of causal and acausal Green's function between the two receivers, the waves obtained by deconvolution represent the elements of the propagator matrix. Finally, we show analytically the extension of the propagator matrix analysis to a lossy layered medium for a special case of normal incidence.

Key words: attenuation, deconvolution, propagator matrix, seismic interferometry.

1 INTRODUCTION

Near-surface properties are useful in quantifying seismic hazards. These properties are important for applications, such as civil engineering and groundwater detection. The variability of the near-surface properties is caused by changes in porosity, permeability, fractures, fluids, compaction, diagenesis and metamorphism (Toksöz *et al.* 1976). The lateral and temporal variations in the near-surface properties are a major cause of poor repeatability of the source radiation pattern (Aritman 2001), and hence reduce the repeatability of time-lapse surveys. Knowledge of these near-surface properties is, hence, crucial for time-lapse monitoring. The local near-surface properties are also required to determine the free-surface reflectivity which is useful to perform wavefield decomposition (Dankbaar 1985; Wapenaar *et al.* 1990). Estimation of the near-surface properties for a lossless homogeneous medium using the propagator matrix and wave-equation inversion is shown for *SH* waves by Trampert *et al.* (1993) and for *P-SV* waves by van Vossen *et al.* (2004).

Seismic interferometry (Elgamal *et al.* 1995; Haddadi & Kawakami 1998a,b; Kawakami & Haddadi 1998; Lobkis & Weaver 2001; Derode *et al.* 2003; Kawakami & Oyunchimeg 2003; Schuster *et al.* 2004; Shapiro & Campillo 2004; Snieder 2004; Wapenaar 2004; Shapiro *et al.* 2005; Wapenaar *et al.* 2005; Snieder *et al.* 2006a) is a technique based on combining signals recorded at different sensors, to estimate the response between them. Until recently cross-correlation is a widely used tool for applying seismic interferometry. Instead of cross-correlation, deconvolution can also be used as a seismic interferometric tool (Snieder & Şafak 2006; Vasconcelos & Snieder 2006). To estimate the near-surface properties, we apply deconvolution to borehole recording of earthquake data. Deconvolution of the incoherent waveforms recorded by the sensors at different depths in the borehole with the recording at the surface results in waves that propagate upwards and downwards along the array. These waves obtained by deconvolution can be used to estimate near-surface properties such as 1-D *P*- and *S*-wave velocity profiles. To get the near-surface properties using deconvolution, it is required to have recording in a borehole with two or more downhole sensors. This method is limited to linear systems and hence cannot be applied in the presence of non-linearity.

Following the study by van Vossen *et al.* (2004), we establish a connection between the waveforms obtained after deconvolution and the elements of the propagator matrix. Further, we show analytically the extension of this analysis to a lossy layered medium for a special case of normal incidence. Section 2 describes the data recorded by a downhole array of sensors during an earthquake in 1994. The application of

deconvolution to these data and connection of the deconvolved waves with the propagator matrix elements for lossy medium are shown in Section 3. Finally, in Section 4 we extend the propagator matrix analysis to a lossy layered medium.

2 EARTHQUAKE DATA RECORDED BY TREASURE ISLAND ARRAY

Downhole arrays of triaxial accelerometers have been installed in California by the California Strong Motion Instrumentation Program (CSMIP). A geotechnical array, known as the Treasure Island array (Shakal *et al.* 2004), was installed in San Francisco Bay by CSMIP in co-operation with other agencies (Graizer *et al.* 2000). The array was installed in 1992 in an area that experienced liquefaction during the Loma Prieta earthquake in 1989. It recorded waveforms excited by an earthquake on 1994 June 26 at 08:42:50.31 (UTC). The earthquake occurred near Richmond, CA and hence, in this paper, is referred to as the Richmond earthquake. It was a 4.0 mag earthquake with focal depth of 6.6 km and epicentral distance of 12.6 km from the sensors in the borehole. The downhole Treasure Island array had six three-component sensors located at different depths with the deepest one at a depth of 104 m. Each of the sensors is located in a different borehole separated by a horizontal distance of 3 m. Graizer *et al.* (2000) and Graizer & Shakal (2004) analysed these data to study site amplification effects as a function of depth. Fig. 1(a) shows the radial component of the acceleration recording of the raw data. In this paper, we restrict our analysis to the body waves that arrive in the time windows in Fig. 1(a) that are labelled as '*P*' and '*S*'.

3 DECONVOLUTION AND PROPAGATOR MATRIX

We use deconvolution to analyse the earthquake data recorded by the Treasure Island Array. The deconvolution of two signals $A(\omega)$ and $B(\omega)$ in the frequency domain is given by

$$D(\omega) = \frac{A(\omega)}{B(\omega)}. \tag{1}$$

The deconvolution may be unstable due to zeros of the spectrum of $B(\omega)$. To avoid this instability, we perform a regularized deconvolution given by

$$D(\omega) = \frac{A(\omega)B^*(\omega)}{|B(\omega)|^2 + \epsilon}, \tag{2}$$

where the asterisk '*' denotes complex conjugate and 'ϵ' refers to a constant added at the denominator to prevent the instability of eq. (1). For our analysis, we choose 'ϵ' to be 1 per cent of the average spectral power of $B(\omega)$.

For the Richmond earthquake data, we deconvolve the waveforms recorded at each of the sensors with the waveforms recorded by the sensor on the surface. Since all three components of the ground motion are recorded at the Treasure Island array, we apply deconvolution to all the three components. For the analysis of the three components, we apply deconvolution to the waves arriving in the *P*- and the *S*-windows separately. Fig. 1(a) shows the time windows we use for defining *P* waves (1.0–4.5 s) and *S* waves (4.5–15.0 s) before applying seismic interferometry.

Fig. 2 shows the transverse component of the waveforms after deconvolving the waves in the *S*-window of the transverse component at each level with the waves in the *S*-window of the transverse component at the surface. The deconvolved waves show an up- and a down-going wave. In order to highlight the waveforms at deeper sensors, we normalize the trace amplitudes with the maximum. Graizer & Shakal (2004) showed the 1-D profile of the *P*-wave velocity and the *S*-wave velocity at the Treasure Island array location using suspension logging and

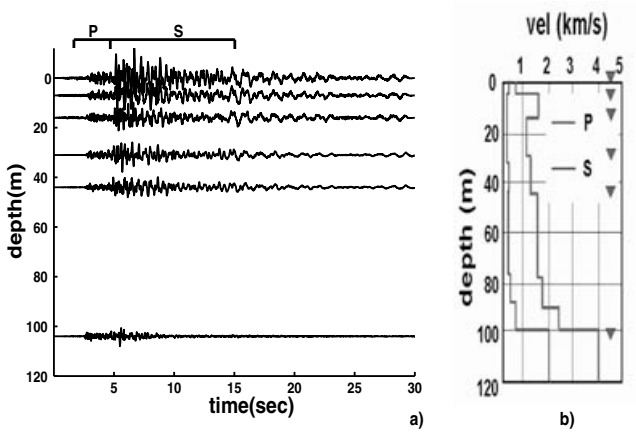

Figure 1. Figure (a) shows the acceleration recording of the radial component of the ground motion recorded by the Treasure Island array near San Francisco during the Richmond earthquake in 1994. The array consists of six three-component sensors located at depths of 0, 7, 16, 31, 44 and 104 m. The time windows used for gating the *P* waves (1.0–4.5 seconds) and the *S* waves (4.5–15.0 seconds) are shown at the top. Figure (b) shows the 1-D velocity profile of the subsurface (Graizer & Shakal 2004) down to 120 m. The triangles show the location of the downhole sensors.

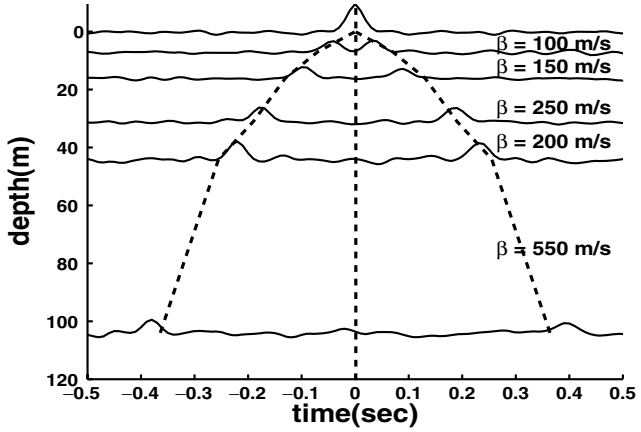

Figure 2. Up- and down-going waves obtained by deconvolving the waveforms in the *S* window of the transverse component of each of the sensors with the waveforms in the *S* window of the transverse component of the sensor on the surface [eq. (2)]. The sloping dashed lines show the traveltime curve of the up- and the down-going *S* waves computed from the *S*-wave velocity model from Graizer & Shakal (2004).

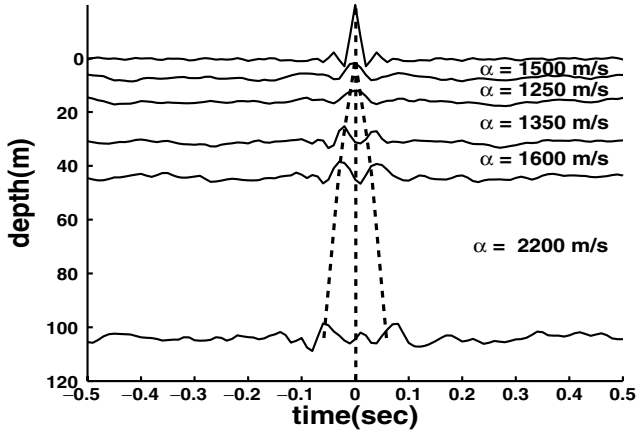

Figure 3. Up- and down-going waves obtained by deconvolving the waveforms recorded by the vertical component of each of the sensors with the waveforms recorded by the vertical component of the sensor on the surface [eq. (2)]. The sloping dashed lines show the traveltime curve of the up- and the down-going *P* waves computed from the *P*-wave velocity model from Graizer & Shakal (2004).

classical downhole measurements (performed by the USGS), as shown in Fig. 1(b). In Fig. 2, we also show the traveltime curve (sloping dashed lines) for up- and down-going *S* waves inferred from the velocity models of Fig. 1(b). Different slopes of the traveltime curve at different depths are due to changes in the shear velocity at these depths. This suggests that the structure around the Treasure Island array is heterogeneous. The traveltime curve agrees with the up- and the down-going waves obtained by deconvolution.

For the vertical component, we apply deconvolution to the waves in both the *P* and the *S* windows. Fig. 3 shows the waveforms after deconvolving the waves recorded at each of the sensors with the waves recorded at the sensor on the surface. Similar to Fig. 2, there is an up- and a down-going wave, but they propagate with velocity higher than the deconvolved waves in Fig. 2. We show the traveltime curve (sloping dashed lines) for up- and down-going *P* waves inferred from this model using the 1-D velocity profile for *P* waves shown in Fig. 1(b). These traveltimes agree with the up- and the down-going waves obtained by deconvolution.

Similar to the transverse component, deconvolution of the waves recorded by the radial component at each of the sensors with the waves recorded at the sensor on the surface also results in an up- and a down-going wave. When the waves in the *S* window are used for deconvolution, it results in an up- and a down-going *S* wave shown in Fig. 4. The sloping dashed line that represents the *S*-wave traveltime curve agrees well with these up- and down-going waves. The agreement of the traveltime curve with the wave-propagation obtained by deconvolution for all the three components suggests that deconvolution can be used to extract near-surface properties such as 1-D *P*- and *S*-wave velocity profiles.

We extracted the *P*- and *S*-wave velocities by deconvolving the waves recorded by a given component at different depths with the same component recording at the surface ($z = 0$). Deconvolution of waves recorded at different depths with the sensor located at a different depth ($z \neq 0$) also gives up- and down-going waves propagating with *P*- or *S*-wave velocities, depending on the component and the time window (Snieder *et al.* 2006b). Similar analysis for multiple recordings at the borehole sensors can be used to get better confidence in the results and estimate on the uncertainty in the 1-D *P*- and *S*-wave velocities. Along with the velocity estimation using the traveltimes, comparison

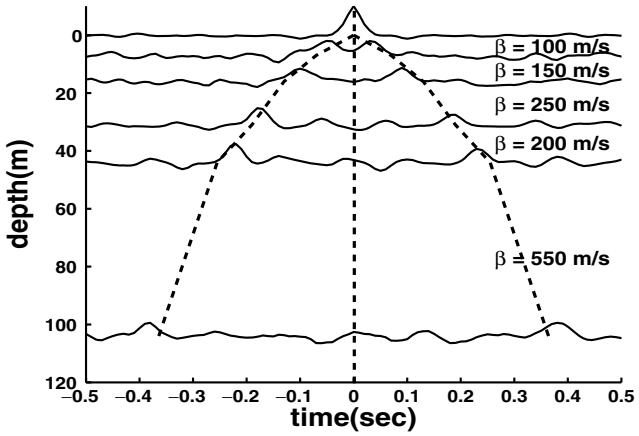

Figure 4. Up- and down-going waves obtained by deconvolving the waveforms in the *S*-window of the radial component of each of the sensors with the waveforms in the *S* window of the radial component of the sensor on the surface [eq. (2)]. The sloping dashed lines show the traveltime curve of the up- and the down-going *S* waves computed from the *S*-wave velocity model from Graizer & Shakal (2004).

of the amplitudes of the up- and the down-going waves at the same depth can be used to estimate the quality factor, a measure of seismic attenuation.

3.1 Analysis with propagator matrix

The signal obtained by correlating two waveforms recorded at different receivers represents the filtered version of the sum of causal and acausal Green's function that characterizes the wave propagation between the two receivers (Lobkis & Weaver 2001; Derode *et al.* 2003; Schuster *et al.* 2004; Shapiro & Campillo 2004; Snieder 2004; Wapenaar 2004; Shapiro *et al.* 2005; Wapenaar *et al.* 2005; Snieder & Şafak 2006). If instead, the two signals are deconvolved, as in our analysis of the Richmond earthquake data, what do the resultant waveforms represent? To address this question, we first treat the connection between the up- and the down-going waves obtained by deconvolution and propagator matrix analysis for *SH* waves that was shown by Trampert *et al.* (1993). For a general layered medium with one of the sensors in a borehole (depth z) and another one at the free surface ($z = 0$), the displacement-stress vector for an *SH* wave at a depth z is expressed as a matrix multiplication of the propagator matrix with the displacement-stress vector at the free surface ($z = 0$) (Aki & Richards 2002). Since the traction at the free surface is zero, this matrix multiplication can be written as

$$\begin{pmatrix} u_y(z,\omega) \\ \sigma_{yz}(z,\omega) \end{pmatrix} = P^{SH}(z,0) \begin{pmatrix} u_y(z=0,\omega) \\ 0 \end{pmatrix}. \tag{3}$$

This is a system of two equations. The first equation can be solved for the *SH* propagator matrix element as

$$P_{11}^{SH}(z,0) = \frac{u_y(z,\omega)}{u_y(z=0,\omega)}. \tag{4}$$

The right-hand side of eq. (4) represents deconvolution in frequency domain. Hence, for *SH* waves, deconvolution of the waveforms recorded at a depth with the waveforms recorded at the surface gives the P_{11} element of the propagator matrix (Trampert *et al.* 1993). Does this also hold true for the *P-SV* waves? To answer this, we consider the frequency domain analysis using propagator matrices by van Vossen *et al.* (2004). Since one of the sensors is at the free surface, the tractions at that sensor vanish. Using this property, they combine the $PSV_{(4*4)}$ and $SH_{(2*2)}$ propagator matrices to give

$$\begin{pmatrix} u_x(z,\omega) \\ u_y(z,\omega) \\ u_z(z,\omega) \end{pmatrix} = P(z,0) \begin{pmatrix} u_x(z=0,\omega) \\ u_y(z=0,\omega) \\ u_z(z=0,\omega) \end{pmatrix}, \tag{5}$$

where

$$P(z,0) = \begin{pmatrix} P_{11}^{PSV}(z,0) & 0 & i\,P_{12}^{PSV}(z,0) \\ 0 & P_{11}^{SH}(z,0) & 0 \\ -i\,P_{21}^{PSV}(z,0) & 0 & P_{22}^{PSV}(z,0) \end{pmatrix}. \tag{6}$$

In eq. (6), $P_{ij}^{PSV/SH}$ stands for ij-element of the $PSV_{(4*4)}$ or $SH_{(2*2)}$ propagator matrix. A derivation of combining the *P-SV* and the *SH* propagator matrices to give eq. (6) is shown in Appendix A.

We show in Appendix B a derivation of the expressions given by van Vossen *et al.* (2004) to express the propagator matrix elements in the measured displacements. The analysis of van Vossen *et al.* (2004) is, however, limited to a homogeneous lossless medium. To establish

the connection between the deconvolved waveforms obtained from the Richmond earthquake and the elements of the propagator matrix, we extend their analysis to a lossy medium.

In the presence of attenuation (Johnston & Toksöz 1981), the propagator matrix elements for a homogeneous medium can be expressed as (Aki & Richards 2002):

$$\begin{aligned} P_{11}^{SH}(z,0) &= \exp[\mathrm{i}\omega q_s z - \xi_s z] + \exp[-\mathrm{i}\omega q_s z + \xi_s z] \\ &= 2\cos[(\omega q_s + \mathrm{i}\xi_s)z], \end{aligned} \tag{7}$$

$$\begin{aligned} P_{11}^{PSV}(z,0) &= 2\beta^2 p^2[\cos\omega q_p z \cosh\xi_p z - \mathrm{i}\sin\omega q_p z \sinh\xi_p z] \\ &\quad + (1-2\beta^2 p^2)[\cos\omega q_s z \cosh\xi_s z - \mathrm{i}\sin\omega q_s z \sinh\xi_s z] \\ &= 2\beta^2 p^2 \cos[(\omega q_p + \mathrm{i}\xi_p)z] + (1-2\beta^2 p^2)\cos[(\omega q_s + \mathrm{i}\xi_s)z], \end{aligned} \tag{8}$$

$$\begin{aligned} \mathrm{i}P_{12}^{PSV}(z,0) &= \frac{p}{q_p}(1-2\beta^2 p^2)[\cos\omega q_p z \sinh\xi_p z - \mathrm{i}\sin\omega q_p z \cosh\xi_p z] \\ &\quad - 2\beta^2 p q_s[\cos\omega q_s z \sinh\xi_s z - \mathrm{i}\sin\omega q_s z \cosh\xi_s z] \\ &= \frac{-\mathrm{i}p}{q_p}(1-2\beta^2 p^2)\sin[(\omega q_p + \mathrm{i}\xi_p)z] + 2\mathrm{i}\beta^2 p q_s \sin[(\omega q_s + \mathrm{i}\xi_s)z], \end{aligned} \tag{9}$$

$$\begin{aligned} -\mathrm{i}P_{21}^{PSV}(z,0) &= \frac{-p}{q_s}(1-2\beta^2 p^2)[\cos\omega q_s z \sinh\xi_s z - \mathrm{i}\sin\omega q_s z \cosh\xi_s z] \\ &\quad - 2\beta^2 p q_p[\cos\omega q_p z \sinh\xi_p z - \mathrm{i}\sin\omega q_p z \cosh\xi_p z] \\ &= \frac{\mathrm{i}p}{q_s}(1-2\beta^2 p^2)\sin[(\omega q_s + \mathrm{i}\xi_s)z] - 2\mathrm{i}\beta^2 p q_p \sin[(\omega q_p + \mathrm{i}\xi_p)z], \end{aligned} \tag{10}$$

$$\begin{aligned} P_{22}^{PSV}(z,0) &= 2\beta^2 p^2[\cos\omega q_s z \cosh\xi_s z - \mathrm{i}\sin\omega q_s z \sinh\xi_s z] \\ &\quad + (1-2\beta^2 p^2)[\cos\omega q_p z \cosh\xi_p z - \mathrm{i}\sin\omega q_p z \sinh\xi_p z] \\ &= 2\beta^2 p^2 \cos[(\omega q_s + \mathrm{i}\xi_s)z] + (1-2\beta^2 p^2)\cos[(\omega q_p + \mathrm{i}\xi_p)z], \end{aligned} \tag{11}$$

where ω is the angular frequency, β the S-wave velocity, p the horizontal slowness, q_p the vertical slowness for P waves, q_s the vertical slowness for S waves, ξ_p the imaginary part of the vertical wavenumber for P waves, and ξ_s the imaginary part of the vertical wavenumber for S waves.

As shown in eqs (7)–(11), for a lossy medium, both the vertical and the horizontal wavenumbers are complex. Complex horizontal wavenumber implies that the horizontal slowness and hence the velocity is complex and frequency-dependent. The associated dispersion is caused by the causality constraint in a lossy medium (Aki & Richards 2002).

In the absence of attenuation, the propagator matrix elements are real. Therefore, P_{11}^{PSV}, P_{11}^{SH} and P_{22}^{PSV} are real and i P_{12}^{PSV} and i P_{21}^{PSV} are imaginary. We show in Appendix B how van Vossen *et al.* (2004) used this to solve eq. (5) for the propagator matrix elements. In the presence of attenuation, however, the propagator matrix elements are complex and hence cannot be determined from these three equations. In that case, it requires more information to express elements of the propagator matrix as a function of the measured displacements. An important parameter in the expressions of the propagator matrix elements is the horizontal slowness p which depends on the angle of incidence. Using the velocity structure of the subsurface down to the hypocentre of the earthquake (Wald *et al.* 1991), we show in Fig. 5 the angle of incidence as a function of the depth. This figure shows that the waves arrive at the surface at near-normal incidence (4°). For normal incidence ($\theta \approx 0°$),

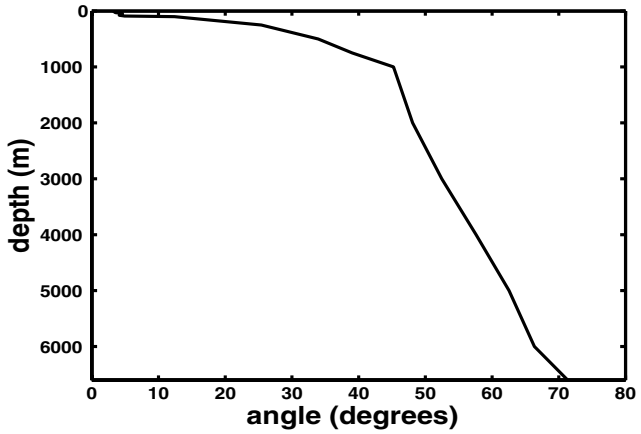

Figure 5. Angle of incidence as a function of depth.

the cross-terms P_{12}^{PSV} and P_{21}^{PSV} in the propagator matrix vanish:

$$P_{12}^{PSV}(z,0) = P_{21}^{PSV}(z,0) = 0. \tag{12}$$

Substituting eq. (12) into eq. (5) gives the following simplified linear system of equations:

$$\begin{pmatrix} u_x(z,\omega) \\ u_y(z,\omega) \\ u_z(z,\omega) \end{pmatrix} = \begin{pmatrix} P_{11}^{PSV}(z,0) & 0 & 0 \\ 0 & P_{11}^{SH}(z,0) & 0 \\ 0 & 0 & P_{22}^{PSV}(z,0) \end{pmatrix} \begin{pmatrix} u_x(z=0,\omega) \\ u_y(z=0,\omega) \\ u_z(z=0,\omega) \end{pmatrix}. \tag{13}$$

Solving the system of eq. (13) gives the propagator elements in terms of displacements:

$$P_{11}^{SH}(z,0) = \frac{u_y(z,\omega)}{u_y(z=0,\omega)}; \quad P_{11}^{PSV}(z,0) = \frac{u_x(z,\omega)}{u_x(z=0,\omega)}; \quad P_{22}^{PSV}(z,0) = \frac{u_z(z,\omega)}{u_z(z=0,\omega)}. \tag{14}$$

The first equation is the same as eq. (4). The other two equations show that for vertically incident *P-SV* waves, we can obtain the propagator matrix elements by applying deconvolution. This holds true for an attenuative medium in a special case of normal incidence. For the Treasure Island data, we perform deconvolution to get the up- and the down-going waves and show in eq. (14) that these deconvolved waves correspond to the propagator matrix elements. In this analysis, one of the sensors is always at the free surface where traction vanishes. If instead the waves recorded at a given depth are deconvolved with the waves recorded at a different depth ($z \neq 0$), the traction values are non-zero and should be incorporated in the analysis.

4 EXTENSION TO A LAYERED MEDIUM

We established the connection between the waveforms obtained after deconvolution and the propagator matrix elements for a lossy homogeneous medium. We extend the propagator matrix analysis to a layered medium. In this section, we show the propagator matrix analysis for a medium consisting of two layers, which can be extended to a multilayered medium. For the two-layer case with one of the sensors at a depth z and another one on the free surface, the displacement and stress for an *SH* wave at a depth z are expressed as a matrix multiplication of the product of propagator matrices corresponding to the two layers with the displacement and stress values at the free surface ($z = 0$) (Aki & Richards 2002). Since the traction at the free surface is zero, this matrix multiplication can be written as

$$\begin{pmatrix} u_y(z,\omega) \\ \sigma_{yz}(z,\omega) \end{pmatrix} = \begin{pmatrix} S_{11} & S_{12} \\ S_{21} & S_{22} \end{pmatrix} \begin{pmatrix} R_{11} & R_{12} \\ R_{21} & R_{22} \end{pmatrix} \begin{pmatrix} u_y(z=0,\omega) \\ 0 \end{pmatrix}, \tag{15}$$

where the matrices **S** and **R** are the *SH* propagator matrices for each layer. We multiply the propagator matrices to get

$$\begin{pmatrix} u_y(z,\omega) \\ \sigma_{yz}(z,\omega) \end{pmatrix} = \begin{pmatrix} (SR)_{11} & (SR)_{12} \\ (SR)_{21} & (SR)_{22} \end{pmatrix} \begin{pmatrix} u_y(z=0,\omega) \\ 0 \end{pmatrix}, \tag{16}$$

which has the same form as eq. (A1) for *SH* waves. If **P** and **Q** are the *P-SV* propagator matrices for the two layers, expression for *P-SV* waves has the same form as eq. (A3). These *SH* and *P-SV* propagator matrices can be combined, as shown in Appendix A, to give

$$\begin{pmatrix} u_x(z,\omega) \\ u_y(z,\omega) \\ u_z(z,\omega) \end{pmatrix} = \begin{pmatrix} (PQ)_{11} & 0 & i(PQ)_{12} \\ 0 & (SR)_{11} & 0 \\ -i(PQ)_{21} & 0 & (PQ)_{22} \end{pmatrix} \begin{pmatrix} u_x(z=0,\omega) \\ u_y(z=0,\omega) \\ u_z(z=0,\omega) \end{pmatrix}, \tag{17}$$

where

$$(SR)_{ij} = \sum_{k=1}^{2} S_{ik} R_{kj}, \tag{18}$$

$$(PQ)_{ij} = \sum_{k=1}^{4} P_{ik} Q_{kj}. \tag{19}$$

The combined matrix has the same form as eq. (A8) in Appendix A. Similar to the case of a homogeneous medium, for a lossless medium the diagonal elements are real and the off-diagonal elements are imaginary. Following the analysis in Appendix B, eq. (17) can be solved for the propagator matrix elements that correspond to a combination of the propagator matrix elements for each layer as shown in eqs (18) and (19).

In the case of a lossy medium, the propagator matrix elements in eq. (17) are complex valued. This makes it impossible to solve eq. (17) for the five elements of the propagator matrix. For the homogeneous case, we assumed normal incidence to simplify the underdetermined system in eq. (5). Let us see if the normal incidence assumption for the layered medium simplifies eq. (17). For normal incidence, the *P-SV* propagator matrix for a homogeneous layer simplifies to

$$P^{PSV} = \begin{pmatrix} P_{11} & 0 & P_{13} & 0 \\ 0 & P_{22} & 0 & P_{24} \\ P_{31} & 0 & P_{33} & 0 \\ 0 & P_{42} & 0 & P_{44} \end{pmatrix}. \tag{20}$$

If we use the *P-SV* propagator matrix for vertically incident waves shown in eq. (20) for multiplication, the terms $(PQ)_{12}$ and $(PQ)_{21}$ in eq. (17) vanish. Hence, the system of equations simplifies to

$$\begin{pmatrix} u_x(z,\omega) \\ u_y(z,\omega) \\ u_z(z,\omega) \end{pmatrix} = \begin{pmatrix} (PQ)_{11} & 0 & 0 \\ 0 & (SR)_{11} & 0 \\ 0 & 0 & (PQ)_{22} \end{pmatrix} \begin{pmatrix} u_x(z=0,\omega) \\ u_y(z=0,\omega) \\ u_z(z=0,\omega) \end{pmatrix}, \tag{21}$$

where, for a two-layer case, the diagonal terms of the matrix in eq. (21) simplify, because of normal incidence, to

$$\begin{aligned} (PQ)_{11} &= P_{11}Q_{11} + P_{13}Q_{31}, \\ (SR)_{11} &= S_{11}R_{11} + S_{12}R_{21}, \\ (PQ)_{22} &= P_{22}Q_{22} + P_{24}Q_{42}. \end{aligned} \tag{22}$$

Hence, for vertically incident waves in a layered medium, the propagator matrix similar to eq. (13) can be obtained by combining the *P-SV* and *SH* propagator matrices, each of which is a combination of the corresponding propagator matrices for each layer as shown in eqs (18) and (19). If each of the layers is homogeneous and incidence is normal, the resultant matrix is diagonal and hence can be solved for the combination of the propagator matrix elements even in the presence of attenuation. Deconvolution applied to the waveforms recorded in a layered medium thus results in the propagator matrix elements of the matrix obtained by combining the *P-SV* and the *SH* matrices of the layered medium.

5 CONCLUSION

We show that deconvolution as a tool for seismic interferometry, applied to data recorded by the Treasure Island array, results in a superposition of up- and down-going *P* and *S* waves. This makes it a valuable tool in estimating the 1-D velocity profile along the recording array. Application of deconvolution to various components of the data results in waves either propagating with *P*- or *S*-wave velocity, and depends on the time window used for gating before applying deconvolution. For both the transverse and radial components, deconvolution of the waves in the *S*-wave window results in the up- and down-going waves with *S*-wave velocity. Deconvolution applied to the vertical component results in up- and down-going waves with the *P*-wave velocity. Finally, we establish a connection of the resultant up- and down-going waves with the propagator matrix elements and show that this type of analysis is possible even in the presence of attenuation as long as we restrict ourselves to normal incidence. We extend the propagator matrix analysis to a layered medium and show that even for a layered medium, the analysis holds in the presence of attenuation for a special case of normal incidence.

ACKNOWLEDGMENTS

We thank the Gamechanger program of Shell International Exploration and Production, Inc., for financial support.

REFERENCES

Aki, K. & Richards, P.G., 2002. *Quantitative Seismology,* 2nd edn, University Science Books, Sausalito.

Aritman, B.C., 2001. Repeatability study of seismic source signatures, *Geophysics,* **66,** 1811–1817.

Dankbaar, J.W.M., 1985. Separation of *P*- and *S*-waves, *Geophys. Prospect.,* **33,** 970–986.

Derode, A., Lacrose, E., Campillo, M. & Fink, M., 2003. How to estimate the Green's function for a heterogeneous medium between two passive sensors? Application to acoustic waves, *Appl. Phys. Lett.,* **83,** 3054–3056.

Elgamal, A.W., Zeghal, M., Tang, H.T. & Stepp, J.C., 1995. Lotung Downhole Array, I: Evaluation of site dynamic properties, *Journal of Geotechnical Engineering,* **121,** No. 4, 350–362.

Graizer, V. & Shakal, A., 2004. Analysis of some of CSMIP strong-motion geotechnical array recordings, *Proceedings of the International Workshop for Site Selection, Installation and Operation of Geotechnical Strong-Motion Arrays: Workshop 1, Inventory of Current and Planner Arrays,* 14 and 15 October 2004, COSMOS, SCEC and USC.

Graizer, V., Cao, T., Shakal, A. & Hipley, P., 2000. Data from downhole arrays instrumented by the California Strong Motion Instrumentation Program in studies of site amplification effects, *Proceedings of the 6th International Conference on Seismic Zonation,* 2000, Palm Springs, California.

Haddadi, H.R. & Kawakami, H., 1998a. Modeling wave propagation by using normalized input-output minimization (NIOM) method for multiple linear systems, *Journal of Structural, Mechanical and Earthquake Engineering,* **15,** No. 1, 29s–39s.

Haddadi, H.R. & Kawakami, H., 1998b. Characteristics of Vertical Component Strong Ground Motion by NIOM (Normalized Input-Output Minimization) Method, *Proceedings of 10th Japan Symposium of Earthquake Engineering*, 1187–1192.

Johnston, D.H. & Toksöz, M.N., 1981. Definitions and Terminology, *Geophysics Reprint Series No.2,* Seismic Wave Attenuation, 1–5.

Kawakami, H. & Haddadi, H.R., 1998. Modeling wave propagation by using normalized input-output minimization (NIOM), *Soil Dynamics and Earthquake Engineering,* **17,** 117–126.

Kawakami, H. & Oyunchimeg, M., 2003. Normalized input-output minimization analysis of wave propagation in buildings, *Engineering Structures,* **25,** 1429–1442.

Lobkis, O.I. & Weaver, R.L., 2001. On the emergence of the Green's function in the correlations of a diffuse field, *Journal of Acoustical Society of America,* **110,** 3011–3017.

Schuster, G.T., Yu, J., Sheng, J. & Rickett, J., 2004. Interferometric/daylight seismic imaging, *Geophys. J. Int.,* **157,** 838–852.

Shakal, A., Hipley, P. & Graizer, V., 2004. CSMIP Instrumented Geotechnical Arrays, *Proceeding of the International Workshop for Site Selection, Installation and Operation of Geotechnical Strong-Motion Arrays: Workshop 1, Inventory of Current and Planned Arrays,* 14 and 15 October 2004, Los Angeles.

Shapiro, N.M. & Campillo, M., 2004. Emergence of broadband Rayleigh waves from correlations of the ambient seismic noise, *Geophys. Res. Lett.,* **31,** L07614, doi10.1029/2004GL019491.

Shapiro, N.M., Campillo, M., Stehly, L. & Ritzwoller, M.H., 2005. High-resolution surface-wave tomography from ambient seismic noise, *Science,* **307,** 1615–1618.

Snieder, R., 2004. Extracting the Green's function from the correlation of coda waves: A derivation based on stationary phase, *Phys. Rev. E.,* **69,** 046610.

Snieder, R. & Şafak, E., 2006. Extracting the building response using seismic interferometry; theory and application to the Millikan Library in Pasadena, California, *Bulletin of Seismological Society of America,* **96,** No. 2, 586–598.

Snieder, R., Wapenaar, K. & Larner, K., 2006a. Spurious multiples in interferometric imaging of primaries, *Geophysics,* **71,** SI111–SI124.

Snieder, R., Sheiman, J. & Calvert, R., 2006b. Equivalence of the virtual source method and wavefield deconvolution in seismic interferometry, *Phys. Rev. E.,* **73,** 066620.

Toksöz, M.N., Cheng, C.H. & Timur, A., 1976. Velocities of seismic waves in porous rocks, *Geophysics,* **41,** 621–645.

Trampert, J., Cara, M. & Frogneux, M., 1993. *SH* propagator matrix and Q_s estimates from borehole- and surface-recorded earthquake data, *Geophys. J. Int.,* **112,** 290–299.

van Vossen, R., Trampert, J. & Curtis, A., 2004. Propagator and wave-equation inversion for near-receiver material properties, *Geophys. J. Int.,* **157,** 796–812.

Vasconcelos, I. & Snieder, R., 2006. Interferometric imaging by deconvolution: Theory and numerical examples, *SEG Expanded Abstracts,* **25,** 2416–2419.

Wapenaar, C.P. A, Herrmann, P., Verschuur, D.J. & Berkhout, A.J., 1990. Decomposition of multicomponent seismic data into primary *P*- and *S*-Wave responses, *Geophys. Prospect.,* **38,** 633–661.

Wapenaar, K., 2004. Retrieving the elastodynamic Green's function of an arbitrary inhomogeneous medium by cross-correlation, *Phys. Rev. Lett.,* **93,** 254301.

Wapenaar, K., Fokkema, J. & Snieder, R., 2005. Retrieving the Green's function by cross-correlation: a comparison of approaches, *Journal of Acoustical Society of America,* **118,** 2783–2786.

Wald, D.J., Helmberger, D.V. & Heaton, T.H., 1991. Rupture Model of the 1989 Loma Prieta earthquake from the inversion of strong-motion and broadband teleseismic data, *Bulletin of the Seismological Society of America,* **81,** No. 5, 1540–1572.

APPENDIX A: DERIVATION OF THE COMBINED PROPAGATOR MATRIX

The displacement and stress for an *SH* wave at a depth z can be expressed as a matrix multiplication of the propagator matrix and the values at the free surface ($z = 0$) (Aki & Richards 2002). Since the traction at the free surface is zero, we can write the multiplication as

$$\begin{pmatrix} u_y(z,\omega) \\ \sigma_{yz}(z,\omega) \end{pmatrix} = P^{SH}(z,0) \begin{pmatrix} u_y(z=0,\omega) \\ 0 \end{pmatrix} \tag{A1}$$

$$\Rightarrow u_y(z,\omega) = P_{11}^{SH}(z,0) u_y(z=0,\omega). \tag{A2}$$

A similar expression for the *P-SV* system is given by

$$\begin{pmatrix} u_x(z,\omega) \\ \mathrm{i}u_z(z,\omega) \\ \sigma_{xz}(z,\omega) \\ \mathrm{i}\sigma_{zz}(z,\omega) \end{pmatrix} = P^{PSV}(z,0) \begin{pmatrix} u_x(z=0,\omega) \\ \mathrm{i}u_z(z=0,\omega) \\ 0 \\ 0 \end{pmatrix} \tag{A3}$$

$$\Rightarrow u_x(z,\omega) = P_{11}^{PSV}(z,0) u_x(z=0,\omega) + \mathrm{i}P_{12}^{PSV}(z,0) u_z(z=0,\omega), \tag{A4}$$

$$\mathrm{i}u_z(z,\omega) = P_{21}^{PSV}(z,0) u_x(z=0,\omega) + \mathrm{i}P_{22}^{PSV}(z,0) u_z(z=0,\omega). \tag{A5}$$

Equations (A2), (A4) and (A5) can be combined to give the following system of equations:

$$\begin{aligned} u_y(z,\omega) &= P_{11}^{SH}(z,0) u_y(z=0,\omega), \\ u_x(z,\omega) &= P_{11}^{PSV}(z,0) u_x(z=0,\omega) + \mathrm{i}P_{12}^{PSV}(z,0) u_z(z=0,\omega), \\ u_z(z,\omega) &= -\mathrm{i}P_{21}^{PSV}(z,0) u_x(z=0,\omega) + P_{22}^{PSV}(z,0) u_z(z=0,\omega). \end{aligned} \tag{A6}$$

This system of equations can be rewritten in matrix form as

$$\begin{pmatrix} u_x(z,\omega) \\ u_y(z,\omega) \\ u_z(z,\omega) \end{pmatrix} = P(z,0) \begin{pmatrix} u_x(z=0,\omega) \\ u_y(z=0,\omega) \\ u_z(z=0,\omega) \end{pmatrix}, \tag{A7}$$

where

$$P(z,0) = \begin{pmatrix} P_{11}^{PSV}(z,0) & 0 & \mathrm{i}P_{12}^{PSV}(z,0) \\ 0 & P_{11}^{SH}(z,0) & 0 \\ -\mathrm{i}P_{21}^{PSV}(z,0) & 0 & P_{22}^{PSV}(z,0) \end{pmatrix} \tag{A8}$$

is the propagator matrix relating the displacements at a depth z with the displacements at the free surface ($z = 0$).

APPENDIX B: SOLVING FOR THE PROPAGATOR MATRIX ELEMENTS IN TERMS OF DISPLACEMENTS

For a homogeneous lossless medium, following are the expressions for the elements of *SH* and *P-SV* propagator matrices, as obtained from Aki & Richards (2002) and simplified to agree with the expressions given by van Vossen *et al.* (2004):

$$\begin{aligned} P_{11}^{SH}(z,0) &= 2\cos(\mathrm{i}\nu z) \\ &= 2\cos(\omega q_s z), \end{aligned} \tag{B1}$$

$$\begin{aligned} P_{11}^{PSV}(z,0) &= 1 + \frac{2\mu}{\omega^2\rho}\left[2k^2\sinh^2\left(\frac{\gamma z}{2}\right) - (k^2+\nu^2)\sinh^2\left(\frac{\nu z}{2}\right)\right] \\ &= 2\beta^2 p^2\cos[\omega(q_p z)] + (1-2\beta^2 p^2)\cos[\omega(q_s z)], \end{aligned} \tag{B2}$$

$$\begin{aligned} P_{12}^{PSV}(z,0) &= \frac{k\mu}{\omega^2\rho}\left[(k^2+\nu^2)\frac{\sinh\gamma z}{\gamma} - 2\nu\sinh\nu z\right] \\ &= \left[\frac{-p(1-2\beta^2 p^2)}{q_p}\right]\sin(\omega q_p z) + 2\beta^2 p q_s\sin(\omega q_s z) \\ \Rightarrow \mathrm{i}P_{12}^{PSV}(z,0) &= \frac{-\mathrm{i}p}{q_p}(1-2\beta^2 p^2)\sin(\omega q_p z) + 2\mathrm{i}\beta^2 p q_s\sin(\omega q_s z), \end{aligned} \tag{B3}$$

$$\begin{aligned} P_{21}^{PSV}(z,0) &= \frac{k\mu}{\omega^2\rho}\left[(k^2+\nu^2)\frac{\sinh\nu z}{\nu} - 2\gamma\sinh\gamma z\right] \\ \Rightarrow -\mathrm{i}P_{21}^{PSV}(z,0) &= \frac{\mathrm{i}p}{q_s}(1-2\beta^2 p^2)\sin(\omega q_s z) - 2\mathrm{i}\beta^2 p q_p\sin(\omega q_p z), \end{aligned} \tag{B4}$$

$$\begin{aligned} P_{22}^{PSV}(z,0) &= 1 + \frac{2\mu}{\omega^2\rho}\left[2k^2\sinh^2\left(\frac{\nu z}{2}\right) - (k^2+\nu^2)\sinh^2\left(\frac{\gamma z}{2}\right)\right] \\ \Rightarrow P_{22}^{PSV}(z,0) &= 2\beta^2 p^2\cos[\omega(q_s z)] + (1-2\beta^2 p^2)\cos[\omega(q_p z)], \end{aligned} \tag{B5}$$

where k is horizontal wavenumber, μ is shear modulus and ρ is density. ν is the vertical wavenumber for S waves and γ is the vertical wavenumber for P waves ($\nu = \omega q_s$ and $\gamma = \omega q_p$). In the absence of attenuation, both ν and γ are real valued.

As shown by van Vossen *et al.* (2004), for lossless medium, we can solve eq. (A7) for the components of the propagator matrix. To solve for the propagator matrix elements, we start with eq. (A7) rewritten as

$$\begin{pmatrix} u_x(z,\omega) \\ u_y(z,\omega) \\ u_z(z,\omega) \end{pmatrix} = \begin{pmatrix} P_{11}^{PSV}(z,0) & 0 & \mathrm{i}P_{12}^{PSV}(z,0) \\ 0 & P_{11}^{SH}(z,0) & 0 \\ -\mathrm{i}P_{21}^{PSV}(z,0) & 0 & P_{22}^{PSV}(z,0) \end{pmatrix} \begin{pmatrix} u_x(z=0,\omega) \\ u_y(z=0,\omega) \\ u_z(z=0,\omega) \end{pmatrix}. \tag{B6}$$

Since the diagonal elements are real and the off-diagonal elements are imaginary, the system of equations in eq. (B6) can be expressed as

$$\begin{aligned} \mathrm{Re}(u_x(z,\omega)) + \mathrm{iIm}(u_x(z,\omega)) &= P_{11}^{PSV}(z,0)[\mathrm{Re}(u_x(z=0,\omega)) + \mathrm{iIm}(u_x(z=0,\omega))] \\ &\quad + \mathrm{i}P_{12}^{PSV}(z,0)[\mathrm{Re}(u_z(z=0,\omega)) + \mathrm{iIm}(u_z(z=0,\omega))], \\ \mathrm{Re}(u_z(z,\omega)) + \mathrm{iIm}(u_z(z,\omega)) &= -\mathrm{i}P_{21}^{PSV}(z,0)[\mathrm{Re}(u_x(z=0,\omega)) + i\,\mathrm{Im}(u_x(z=0,\omega))] \\ &\quad + P_{22}^{PSV}(z,0)[\mathrm{Re}(u_z(z=0,\omega)) + \mathrm{iIm}(u_z(z=0,\omega))]. \end{aligned} \tag{B7}$$

In order to solve for the propagator matrix elements, we equate the real and imaginary parts to give the following equations:

$$\begin{aligned} \mathrm{Re}(u_x(z,\omega)) &= P_{11}^{PSV}(z,0)\mathrm{Re}(u_x(z=0,\omega)) - P_{12}^{PSV}(z,0)\mathrm{Im}(u_z(z=0,\omega)), \\ \mathrm{Im}(u_x(z,\omega)) &= P_{11}^{PSV}(z,0)\mathrm{Im}(u_x(z=0,\omega)) + P_{12}^{PSV}(z,0)\mathrm{Re}(u_z(z=0,\omega)), \\ \mathrm{Re}(u_z(z,\omega)) &= P_{21}^{PSV}(z,0)\mathrm{Im}(u_x(z=0,\omega)) + P_{22}^{PSV}(z,0)\mathrm{Re}(u_z(z=0,\omega)), \\ \mathrm{Im}(u_z(z,\omega)) &= -P_{21}^{PSV}(z,0)\mathrm{Re}(u_x(z=0,\omega)) + P_{22}^{PSV}(z,0)\mathrm{Im}(u_z(z=0,\omega)). \end{aligned} \tag{B8}$$

Solving this system of equations for the elements of the propagator matrix gives

$$P_{11}^{SH}(z,0) = \frac{u_y(z,\omega)}{u_y(z=0,\omega)},$$

$$P_{11}^{PSV}(z,0) = \frac{\mathrm{Re}(u_x(z,\omega))\mathrm{Re}(u_z(z=0,\omega)) + \mathrm{Im}(u_x(z,\omega))\mathrm{Im}(u_z(z=0,\omega))}{\mathrm{Re}(u_x(z=0,\omega))\mathrm{Re}(u_z(z=0,\omega)) + \mathrm{Im}(u_x(z=0,\omega))\mathrm{Im}(u_z(z=0,\omega))},$$

$$P_{12}^{PSV}(z,0) = \frac{\mathrm{i}[\mathrm{Re}(u_x(z=0,\omega))\mathrm{Im}(u_x(z,\omega)) - \mathrm{Im}(u_x(z=0,\omega))\mathrm{Re}(u_x(z,\omega))]}{\mathrm{Re}(u_x(z=0,\omega))\mathrm{Re}(u_z(z=0,\omega)) + \mathrm{Im}(u_x(z=0,\omega))\mathrm{Im}(u_z(z=0,\omega))},$$

$$P_{21}^{PSV}(z,0) = \frac{-\mathrm{i}[\mathrm{Re}(u_z(z=0,\omega))\mathrm{Im}(u_z(z,\omega)) - \mathrm{Im}(u_z(z=0,\omega))\mathrm{Re}(u_z(z,\omega))]}{\mathrm{Re}(u_x(z=0,\omega))\mathrm{Re}(u_z(z=0,\omega)) + \mathrm{Im}(u_x(z=0,\omega))\mathrm{Im}(u_z(z=0,\omega))},$$

$$P_{22}^{PSV}(z,0) = \frac{\mathrm{Re}(u_x(z=0,\omega))\mathrm{Re}(u_z(z,\omega)) + \mathrm{Im}(u_x(z=0,\omega))\mathrm{Im}(u_z(z,\omega))}{\mathrm{Re}(u_x(z=0,\omega))\mathrm{Re}(u_z(z=0,\omega)) + \mathrm{Im}(u_x(z=0,\omega))\mathrm{Im}(u_z(z=0,\omega))}. \quad \text{(B9)}$$

Hence, for a homogeneous medium, the propagator matrix elements can be expressed in terms of displacements at the depth of interest z and at the free surface ($z = 0$).